ARTICLES
PUBLISHED ONLINE: 18 MAY 2014 | DOI: 10.1038/NCHEM.1956
nature chemistry

Oxidation of ethane to ethanol by N_2O in a metal–organic framework with coordinatively unsaturated iron(II) sites

Dianne J. Xiao[1], Eric D. Bloch[1], Jarad A. Mason[1], Wendy L. Queen[2], Matthew R. Hudson[3], Nora Planas[4], Joshua Borycz[4], Allison L. Dzubak[4], Pragya Verma[4], Kyuho Lee[2], Francesca Bonino[5], Valentina Crocellà[5], Junko Yano[6], Silvia Bordiga[5], Donald G. Truhlar[4], Laura Gagliardi[4], Craig M. Brown[3,7] and Jeffrey R. Long[1,8]*

Enzymatic haem and non-haem high-valent iron–oxo species are known to activate strong C–H bonds, yet duplicating this reactivity in a synthetic system remains a formidable challenge. Although instability of the terminal iron–oxo moiety is perhaps the foremost obstacle, steric and electronic factors also limit the activity of previously reported mononuclear iron(IV)–oxo compounds. In particular, although nature's non-haem iron(IV)–oxo compounds possess high-spin $S = 2$ ground states, this electronic configuration has proved difficult to achieve in a molecular species. These challenges may be mitigated within metal–organic frameworks that feature site-isolated iron centres in a constrained, weak-field ligand environment. Here, we show that the metal–organic framework Fe_2(dobdc) (dobdc^{4-} = 2,5-dioxido-1,4-benzenedicarboxylate) and its magnesium-diluted analogue, $Fe_{0.1}Mg_{1.9}$(dobdc), are able to activate the C–H bonds of ethane and convert it into ethanol and acetaldehyde using nitrous oxide as the terminal oxidant. Electronic structure calculations indicate that the active oxidant is likely to be a high-spin $S = 2$ iron(IV)–oxo species.

The selective and efficient conversion of light alkanes into value-added chemicals remains an outstanding challenge with tremendous economic and environmental impacts[1,2], especially given the recent worldwide increase in natural gas reserves[3]. In nature, C–H functionalization is carried out by copper and iron metalloenzymes, which activate dioxygen and facilitate two- or four-electron oxidations of organic substrates[4–7] through metal-oxo intermediates. Duplicating this impressive reactivity in synthetic systems has been the focus of intense research. In particular, iron(IV)–oxo complexes have now been characterized structurally in various geometries (octahedral, trigonal bipyramidal) and spin states ($S = 1$, $S = 2$), and have proved to be competent catalysts for a variety of oxygenation reactions[8,9].

However, in the absence of a protective protein superstructure, terminal iron–oxo species are highly susceptible to a variety of decomposition pathways, which include dimerization to form oxo-bridged diiron complexes, intramolecular ligand oxidation and solvent oxidation[10]. Tethering a molecular iron species to a porous solid support, such as silica or polystyrene, could potentially prevent many of these side-reactions. In practice, however, complexes heterogenized in this manner are difficult to characterize using available techniques, and additional problems associated with steric crowding, site inaccessibility and metal leaching inevitably arise[11,12]. Iron cations can also be incorporated into zeolites, either as part of the framework or at extraframework sites, to produce reactive iron centres that have no direct molecular analogue. Fe-ZSM-5 (ZSM = Zeolite Socony Mobil), for example, has been shown to oxidize methane to methanol stoichiometrically when pretreated with nitrous oxide[13]. However, characterization of these materials is nontrivial because of the presence of multiple iron species, and the nature of the active sites in Fe-ZSM-5 remains largely a matter of speculation[14].

The use of a metal–organic framework (MOF) to support isolated terminal iron–oxo moieties is a currently unexplored yet highly promising area of research. The high surface area, permanent porosity, chemical and thermal stability, and synthetic tunability displayed by many of these materials makes them appealing in this regard. Additionally, MOFs are typically highly crystalline with well-defined metal centres suited for characterization by single-crystal and/or powder-diffraction techniques. Furthermore, although molecular iron(IV)–oxo complexes generally utilize nitrogen-based chelating ligands, the metal cations in MOFs are often ligated by weaker-field ligands, such as carboxylates and aryl oxides, which are constrained in their coordination position by the extended framework structure. Thus, in addition to increased stability, terminal oxos in these materials might also have novel electronic properties and reactivity imparted by their unique coordination environment.

Herein we show that the high-spin iron(II) centres within Fe_2(dobdc) (dobdc^{4-} = 2,5-dioxido-1,4-benzenedicarboxylate) can activate N_2O, most likely forming a transient, high-spin iron(IV)–oxo intermediate, which rapidly reacts to afford $Fe_2(OH)_2$(dobdc).

[1]Department of Chemistry, University of California, Berkeley, California 94720-1460, USA, [2]The Molecular Foundry, Lawrence Berkeley National Laboratory, Berkeley, California 94720-1460, USA, [3]Center for Neutron Research, National Institute of Standards and Technology, Gaithersburg, Maryland 20899, USA, [4]Department of Chemistry, Chemical Theory Center, and Supercomputing Institute, University of Minnesota, Minneapolis, Minnesota, 55455-0431, USA, [5]Department of Chemistry, NIS and INSTM Reference Centres, University of Turin, I-10135 Torino, Italy, [6]Physical Biosciences Division, Lawrence Berkeley National Laboratory, Berkeley, California 94720-1460, USA, [7]Department of Chemical Engineering, University of Delaware, Newark, Delaware 19716, USA, [8]Materials Sciences Division, Lawrence Berkeley National Laboratory, Berkeley, California 94720, USA. *e-mail: jrlong@berkeley.edu

Significantly, the magnesium-diluted analogue, $Fe_{0.1}Mg_{1.9}$(dobdc), is found to oxidize ethane into ethanol in the presence of N_2O under mild conditions.

Results and discussion

Nitrous oxide coordination and activation. Of the three-dimensional iron(II)-containing MOFs shown to be stable to desolvation[15–18], few possess coordinatively unsaturated metal centres in a single, well-defined environment. The compound Fe_2(dobdc) (**1**), also known as Fe-MOF-74 or CPO-27-Fe, is rare in this regard, as the hexagonal channels of the framework are lined with a single type of square pyramidal iron(II) site (see Fig. 1a). The high density and redox-active nature of these open metal sites engender excellent O_2/N_2 and hydrocarbon separation properties[18,19]. However, with respect to the reactivity of the framework, only the hydroxylation of benzene into phenol and the oxidation of methanol into formaldehyde have been reported[20,21]. Thus, we embarked on a study of its reactivity towards nitrous oxide, a gaseous two-electron oxidant and O-atom transfer agent that is widely employed in industry, anticipating the generation of a highly reactive iron(IV)–oxo species capable of oxidizing strong C–H bonds.

We first investigated the binding of nitrous oxide to **1** under conditions in which the Fe–N_2O interaction is reversible. Experimental studies on the coordination chemistry of N_2O are scarce, as metal–N_2O adducts are challenging to synthesize because of the poor σ-donating and π-accepting properties of the molecule[22]. Indeed, of the several proposed binding modes, only one (end-on, η^1-N) has been structurally characterized in a molecular complex[23]. To establish the coordination mode of N_2O in **1**, powder neutron-diffraction data, which are very sensitive to the atomic assignment of O and N, were collected on a sample dosed with various loadings of N_2O. At low loadings, the best fit was an average of approximately 60% η^1-O and 40% η^1-N coordination, with Fe–N_2O distances of 2.42(3) and 2.39(3) Å, respectively. In both cases, a bent Fe–N_2O angle close to 120° was observed (see Fig. 1b). Density functional theory (DFT) studies of N_2O-bound **1** using the M06 functional[24] show excellent agreement with experiment (see Supplementary Fig. 20). Furthermore, these calculations predict the η^1-O coordination mode to be favoured over the η^1-N mode by just 1.1 kJ mol^{-1} (see Supplementary Tables 17 and 22). This is consistent with the nearly equal population split observed, although the magnitude of the difference in energy is smaller than the potential error associated with the calculations.

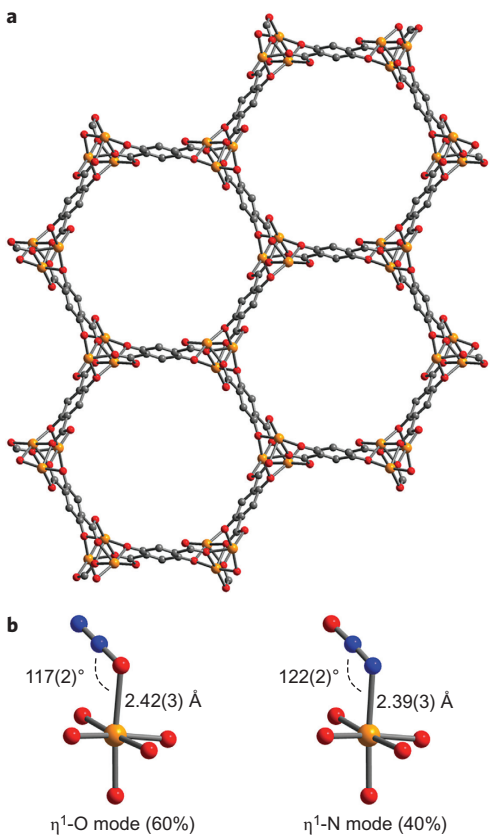

Figure 1 | Structure of bare and N_2O-dosed Fe_2(dobdc) (1). a, Structure of Fe_2(dobdc), showing hexagonal channels lined with five-coordinate iron(II) sites. The view is down the *c* axis, along the helical chains of iron(II) ions. **b**, Experimental structures for N_2O binding in Fe_2(dobdc), solved from powder neutron diffraction data collected at 10 K. The molecule binds with a bent Fe–N_2O angle, with a mixture of 60% η^1-O coordination and 40% η^1-N coordination (for a comparison of calculated structures with experimental ones, see Supplementary Fig. 20). Orange, grey, dark blue and red spheres represent Fe, C, N and O, respectively; H atoms are omitted for clarity.

Although η^1-O coordination with a bent Fe–O–N angle has been proposed in a variety of systems ranging from isolated metal atoms to iron zeolites[22,25,26], η^1-N coordination with a bent Fe–N–N angle is much more unusual. It suggests little π-back-bonding from the metal *d* orbitals into the π^* of N_2O. This is in contrast to previously reported vanadium– and ruthenium–N_2O adducts, which have linear metal–N–N–O geometries and for which π-interactions have been invoked as significant contributors to the stability of the complexes[23,27–29]. The bent geometry, long Fe–N_2O bond length and mixed N and O coordination indicate that N_2O is bound only weakly to the iron(II) centres in the framework, a hypothesis corroborated by *in situ* transmission-mode infrared spectroscopy. Spectra collected on a thin film of **1** dosed at room temperature with N_2O display a maximum at 2,226 cm^{-1}, which is very close to the fundamental ν(N–N) transition for unbound N_2O (2,224 cm^{-1}) and suggests a physically adsorbed phase with little to no perturbation of the N_2O molecule (see Supplementary Fig. 1). As expected, this interaction is fully reversible, and the band disappears completely under an applied vacuum. Consistent with these experimental results, DFT studies calculate binding energies of 45.6 and 44.5 kJ mol^{-1} for the η^1-O and η^1-N modes, respectively, with a natural bond order analysis[30] that shows weak back-bonding in both configurations (see Supplementary Table 23).

On heating the N_2O-dosed framework to 60 °C, the material undergoes a drastic colour change from bright green to dark red–brown, suggestive of oxidation. In addition, *in situ* infrared studies using CO as a probe molecule show that the open metal sites, which coordinate CO strongly, have been almost entirely consumed (see Supplementary Fig. 9). Characterization of the resulting product is consistent with the formulation $Fe_2(OH)_2$(dobdc) (**2**), in which each iron centre is in the +3 oxidation state and bound to a terminal hydroxide anion (see Fig. 2a). Compound **2** is likely to be formed via a fleeting iron–oxo intermediate, which rapidly undergoes hydrogen-atom abstraction, although the source of the hydrogen atom has not yet been determined. Mössbauer spectroscopy was used to probe the local environment of the iron centres in the oxidized material. The ^{57}Fe Mössbauer spectrum of **2** consists of a doublet characterized by an isomer shift (δ) of 0.40(2) mm s^{-1} and a quadrupole splitting ($|\Delta E_Q|$) of 0.96(1) mm s^{-1} (see Fig. 2c). The isomer shift for the iron centres in **2** is similar to the parameters obtained for the peroxide-coordinated iron(III) centres in $Fe_2(O_2)$(dobdc) (ref. 18), and is consistent with other high-spin haem and non-haem iron(III) species[31–33]. In addition, the infrared spectrum of **2** shows the appearance of two new bands as compared to the unoxidized framework, which we assign as Fe–OH (667 cm^{-1}) and O–H (3,678 cm^{-1}) vibrations. These bands shift to 639 and

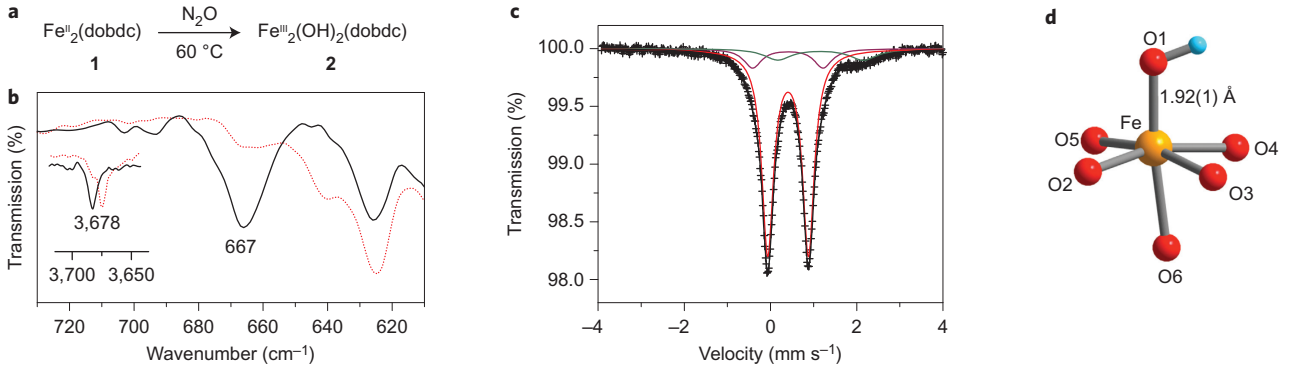

Figure 2 | Preparation, spectroscopic characterization and structure of $Fe_2(OH)_2(dobdc)$. a, Reaction scheme for the preparation of $Fe_2(OH)_2(dobdc)$ (**2**) from $Fe_2(dobdc)$ (**1**). **b**, Infrared spectrum of partially oxidized samples of $Fe_2(OH)_{0.6}(dobdc)$ (**2′**) (black line) and $Fe_2(^{18}OH)_{0.6}(dobdc)$ (dotted red line). The peaks at 667 and 3,678 cm^{-1} shift to 639 and 3,668 cm^{-1}, respectively, when $N_2{}^{18}O$ is used, which confirms that these are, indeed, new bands derived from N_2O and not simply shifted framework bands. This also strongly supports the assignment of these peaks as Fe–OH and O–H vibrations. **c**, Mössbauer spectrum of **2**, with the fit in black. The red component has parameters consistent with high-spin Fe(III) ($\delta = 0.40(2)$ mm s^{-1}, $|\Delta E_Q| = 0.96(1)$ mm s^{-1}, area = 80(2)%). A minor component (green) is assigned as unreacted Fe(II) sites, and another minor component (purple) is assigned as an amorphous Fe(III) decomposition product. **d**, The structure of **2** obtained from powder X-ray diffraction data (100 K). The Fe–OH bond distance of 1.92(1) Å is consistent with that in previously reported Fe(III)–OH compounds. The hydrogen atom on the hydroxide is shown for clarity, but was not found from the diffraction data. Selected interatomic distances (Å) for **2**: Fe–O1 = 1.92(1), Fe–O2 = 2.01(1), Fe–O3 = 2.08(1), Fe–O4 = 2.04(1), Fe–O5 = 2.04(1), Fe–O6 = 2.20(1), Fe–Fe = 3.16(1). Orange, red and light blue spheres represent Fe, O and H, respectively.

3,668 cm^{-1}, respectively, when $N_2{}^{18}O$ is employed for the oxidation; the observed differences of 28 and 10 cm^{-1} are very close to the theoretical isotopic shifts of 27 and 12 cm^{-1} predicted by a simple harmonic oscillator model (see Fig. 2b). Partial oxidation of the framework was achieved by heating at 35 °C for 12 hours, which led to the formation of $Fe_2(OH)_{0.6}(dobdc)$ (**2′**), which has a similar infrared spectrum (although the bands associated with Fe–OH are less intense) and Mössbauer parameters (see Supplementary Table 9).

The framework maintains both crystallinity and porosity after oxidation, with a Brunauer–Emmett–Teller (BET) surface area of 1,013 m^2 g^{-1} and a Langmuir surface area of 1,171 m^2 g^{-1}. Rietveld analysis of powder X-ray diffraction data collected at 100 K on **2** firmly established the presence of a new Fe–O bond, but did not reveal whether a hydrogen atom was present. However, the Fe–OH bond distance of 1.92(1) Å is consistent with the bond lengths of previously reported octahedral iron(III)–hydroxide complexes (1.84–1.93 Å) (see Fig. 2d)[34]. In addition, the *trans* Fe–O_{axial} bond is slightly elongated (Fe–O_{axial} = 2.20(1) Å, average Fe–$O_{equatorial}$ = 2.04(1) Å), with the iron centre shifted slightly (by 0.23(1) Å) out of the plane of the four equatorial oxygen atoms. Extended X-ray absorption fine structure (EXAFS) analysis of the same sample, as well as periodic DFT calculations, provided bond lengths that are consistent with those obtained from the diffraction data (see Supplementary Table 8).

Surprisingly, the iron(III)–hydroxide species is capable of activating weak C–H bonds. When the partially oxidized sample **2′** was exposed to 1,4-cyclohexadiene (C–H bond dissociation energy of 322 kJ mol^{-1})[35] at room temperature, benzene was produced as the sole product in quantitative yield. In the process, the framework converted entirely back to iron(II), as determined by Mössbauer spectroscopy. Such reactivity is rare, but not unprecedented, for iron(III)–hydroxide compounds. For instance, lipoxygenase, an enzyme that converts 1,4-dienes into alkyl hydroperoxides, is believed to proceed through a non-haem ferric hydroxide intermediate[5] and several molecular lipoxygenase mimics have also been reported to activate the C–H bond of 1,4-cyclohexadiene and other 1,4-dienes[36,37]. However, the oxidizing power of **2** and **2′** is limited, and no reaction was observed with less-activated C–H bonds.

Oxidation of ethane to give ethanol. As the isolation of an iron(III)–hydroxide product from a reaction that employs a two-electron oxidant strongly suggests the intermediacy of an iron(IV)–oxo species, we next carried out the oxidation in the presence of a hydrocarbon substrate that contained stronger C–H bonds, specifically ethane (C–H bond dissociation energy of 423 kJ mol^{-1}), hoping to intercept the oxo species before its decay. Indeed, flowing an N_2O:ethane:Ar mixture (10:25:65) over the framework at 75 °C led to the formation of various ethane-derived oxygenates, which included ethanol, acetaldehyde, diethyl ether and other ether oligomers, as determined by ^{1}H NMR spectroscopy of the extracted products (Supplementary Fig. 21). The formation of ether products is not unprecedented, as N_2O-treated Fe-ZSM-5 forms a small amount of dimethyl ether in addition to methanol when exposed to methane, via a mechanism proposed to involve methyl radicals as well as multiple iron sites[38]. We hypothesized that the complex mixture of products was related to the close proximity of reactive iron centres, which are 8.13(2) Å and 6.84(1) Å apart across and along a channel, respectively, in **1**. To avoid oligomerization and overoxidation, a mixed-metal MOF, $Fe_{0.1}Mg_{1.9}(dobdc)$ (**3**), in which the iron(II) sites are diluted with redox-inactive magnesium(II) centres, was synthesized. The BET surface area of 1,670 m^2 g^{-1} for this material falls between the surface areas of the pure iron and pure magnesium frameworks (1,360 and 1,800 m^2 g^{-1}, respectively). Although determining the exact distribution of metal centres in heterometallic MOFs is challenging, the unit-cell parameters of **3** are between those of $Fe_2(dobdc)$ and $Mg_2(dobdc)$ (see Supplementary Table 10), which suggests the formation of a solid solution rather than a mixture of two separate phases. Additionally, the Mössbauer spectrum of **3** shows sharp doublets with a significantly different quadrupole splitting to that of the all-iron analogue (2.25(1) mm s^{-1} versus 2.02(1) mm s^{-1} in $Fe_2(dobdc)$; see Supplementary Table 9), which indicates that the iron centres in the magnesium-diluted framework are in an altered, but uniform, environment. Thus, **3** is possibly best described as containing either isolated iron centres or short multiiron segments dispersed evenly throughout a magnesium-based framework.

Exposure of **3** to N_2O and ethane under the same flow-through conditions yielded the exclusive formation of ethanol and

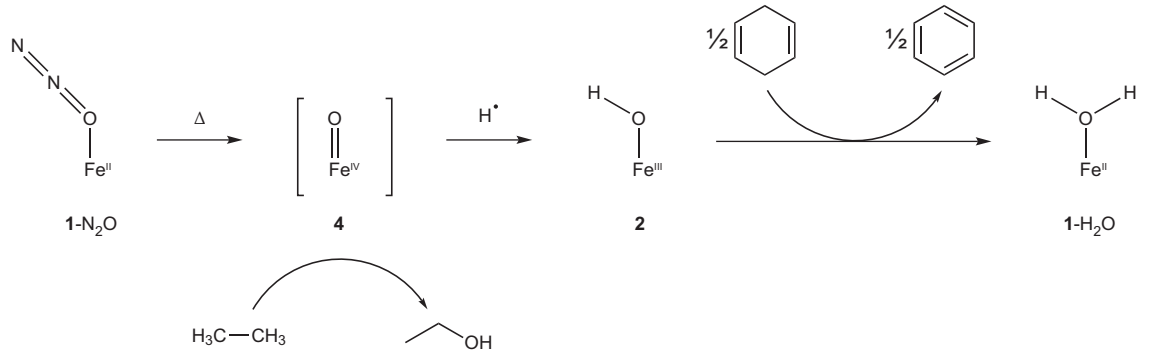

Figure 3 | N_2O activation and reactivity of Fe_2(dobdc) in the oxidation of ethane and 1,4-cyclohexadiene. Heating of N_2O-bound Fe_2(dobdc) (**1**-N_2O) to 60 °C results in the formation of a transient high-spin Fe(IV)–oxo species (**4**), which can react with the strong C–H bonds of ethane. In the absence of a hydrocarbon substrate, the Fe(IV)–oxo quickly decays via hydrogen-atom abstraction into an Fe(III)–hydroxide (**2**), which is isolable and well characterized. This hydroxide species can react with weak C–H bonds, such as those in 1,4-cyclohexadiene, to form benzene and H_2O-bound Fe_2(dobdc) (**1**-H_2O).

acetaldehyde in a 10:1 ratio (as shown in the ^{1}H NMR spectrum in Supplementary Fig. 22), albeit in low yield (60% with respect to iron). Gas chromatography analysis of the headspace revealed no ethanol, acetaldehyde or CO, which suggests the products remained bound to the framework (either at open iron or open magnesium sites), and may explain the high ethanol selectivity. Although the framework was still highly crystalline after N_2O/ethane treatment, Mössbauer spectroscopy revealed that roughly 90% of the iron centres decayed into a species with similar spectral parameters as those of **2** (see Supplementary Fig. 18 and Supplementary Table 9). We propose that the formation of iron(III)–hydroxide or –alkoxide decay products prematurely halts the catalytic cycle, which leads to substoichiometric yields of hydroxylated product (see Fig. 3). As glass can be a source of H atoms, the reaction was subsequently repeated in a batch mode, rather than flow-through, in a Teflon-lined stainless-steel bomb. This produced both higher yields with respect to iron (turnover number = 1.6) and selectivities (25:1 ethanol:acetaldehyde). Though the yield based on ethane (roughly 1%) is still too low for practical purposes, this demonstrates that the system can, indeed, be modestly catalytic if competing substrates are excluded.

Electronic-structure calculations. As the high reactivity of the iron–oxo species precluded isolation in both Fe_2(dobdc) and its magnesium-diluted analogue, electronic structure calculations were performed on $Fe_2(O)_2$(dobdc) (**4**) to gain insight into the geometric and electronic structure of iron–oxo units supported within the framework. First, periodic PBE + U[39,40] geometry optimizations were performed on **4** for the singlet, triplet and quintet spin states. A quintet ground state was predicted, with a short Fe–O bond length of 1.64 Å, consistent with that of previously reported iron(IV)–oxo complexes (see Fig. 4 and Supplementary Table 11)[8]. The periodic structure was then truncated to an 89-atom model cluster[41,42] that contained three metal centres, six organic linkers and an oxo moiety to facilitate calculations using more accurate methods. The cluster calculations were simplified by replacing the two peripheral iron(II) centres with closed-shell zinc(II) centres, which have the same charge and a similar ionic radius to iron(II) and magnesium(II) cations (see Supplementary Fig. 19). The geometry of this cluster was then optimized, with all atoms except for the central iron and its first coordination sphere frozen at the coordinates from the periodic PBE + U optimization. As shown in Table 1, the M06//M06-L[24] calculations also predict a quintet ground state. Further calculations were performed with several other exchange-correlation functionals, and in each case the ground state was found to be a quintet (see Supplementary Tables 11–16). Similar results were obtained when the Zn(II) centres in the 89-atom cluster were replaced with Mg(II) centres (see Supplementary Tables 20 and 21).

The electronic structure of the cluster model of **4** was examined further with single-point multiconfigurational complete active space (CASSCF) calculations followed by second-order perturbation theory (CASPT2)[43,44]. Again, the ground state is predicted to be the quintet state (see Table 1 and Supplementary Table 18). Both M06//M06-L and CASPT2//PBE yield a spin density of ~3.7 on iron, consistent with four unpaired spins localized mainly on the metal (see Supplementary Tables 13 and 19). Density functional and CASPT2 calculations were also performed on the cluster model of **2**; all calculations led to a high-spin sextet ground state for the iron(III) centre (see Supplementary Tables 11–16 and Supplementary Table 18).

Although spectroscopic and theoretical studies have long attributed the reactivity of non-haem enzymatic and synthetic iron(IV)–oxo

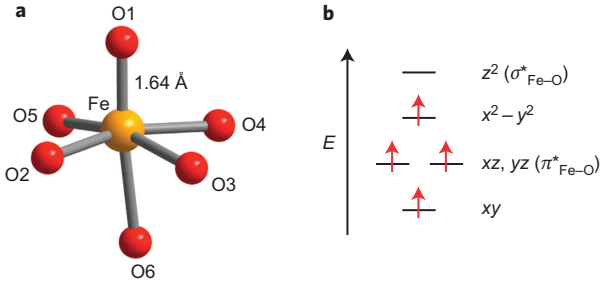

Figure 4 | Structure and qualitative MO diagram of $Fe_2(O)_2$(dobdc) (4). **a**, DFT and CASSCF/PT2 studies predict a short iron–oxo bond (1.64 Å) for $Fe_2(O)_2$(dobdc) (**4**). Selected interatomic distances (Å) for **4**: Fe–O1 = 1.638; Fe–O2 = 2.004; Fe–O3 = 2.127; Fe–O4 = 2.019; Fe–O5 = 2.054; Fe–O6 = 2.140. Orange and red spheres represent Fe and O respectively. **b**, DFT and CASSCF/PT2 studies all predict a high-spin $S = 2$ ground state for iron(IV)–oxo compounds installed in the Fe_2(dobdc) framework.

Table 1 | Calculated relative energies (kJ mol^{-1}) of the cluster model of 4.

S	M06//M06-L	CASPT2//PBE
0	210.6	249.4
1	136.4	127.6
2	0.0	0.0

Density functional and CASPT2 calculations were performed on a truncated model of $Fe_2(O)_2$(dobdc) (**4**) that contained a central iron atom, two peripheral Zn(II) atoms (to replicate the rigid framework structure) and six organic linkers (see Supplementary Fig. 19). The relative energies of the cluster models in different spin states are given here. By both methods, the quintet state ($S = 2$) is the calculated ground state.

complexes to a quintet spin state[45], only a handful of mononuclear high-spin iron(IV)–oxo species have been characterized[46–49], and all but one exhibit a trigonal bipyramidal coordination geometry[50]. In these systems, the oxo moiety is either extremely unstable ($[Fe(O)(H_2O)_5]^{2+}$, for example, has a half-life of roughly ten seconds) or inaccessible to substrates because of bulky ligand scaffolds, which lead to sluggish reactivity. However, the Fe_2(dobdc) framework features sterically accessible, site-isolated metal centres entrenched in a weak-field ligand environment. Utilizing these two properties, it is possible not only to generate such a species, albeit fleetingly, but also to direct it towards the facile activation of one of the strongest C–H bonds known.

Concluding remarks

The foregoing results demonstrate, through reactivity studies, detailed characterizations of decay products and theoretical calculations, that the iron-based MOFs Fe_2(dobdc) and $Fe_{0.1}Mg_{1.9}$(dobdc) are very likely to be capable of supporting fleeting iron(IV)–oxo species that possess an unusual $S = 2$ spin state. With this, Fe_2(dobdc) has now been shown to stabilize iron–superoxo, –peroxo, –hydroxo and –oxo intermediates, which highlights the promise of MOFs both as catalysts and as scaffolds for interrogating reactive metal species. Future work will focus on (1) further exploring the reactivity of Fe_2(dobdc) and its expanded analogues towards ethane and other hydrocarbon substrates, as well as continued efforts to isolate the iron-oxo species, (2) the use of dioxygen as the terminal oxidant in such systems and (3) the design, synthesis and reactivity of other MOFs with coordinatively unsaturated iron sites.

Methods

Synthesis of $Fe_2(OH)_{0.6}$(dobdc) (2′) and $Fe_2(OH)_2$(dobdc) (2). An evacuated Schlenk flask that contained fully desolvated Fe_2(dobdc) (100 mg, 0.33 mmol) was placed under an atmosphere of 30% N_2O and 70% N_2. The flask was immersed in an oil bath, and the temperature was increased by 10 °C every 12 hours, from 25 °C up to 60 °C, to obtain $Fe_2(OH)_2$(dobdc) as a dark red–brown solid. When the reaction was stopped after 12 hours at 35 °C, partially oxidized $Fe_2(OH)_{0.6}$(dobdc) (as determined by Mössbauer spectroscopy) was obtained. Analytical: $C_8H_4Fe_2O_8$ calculated, C, 28.28, H, 1.19; found, C, 29.18, H, 1.16. Infrared (solid attenuated total reflection (ATR)) spectroscopy: 3,679 (m), 1,532 (s), 1,450 (s), 1,411 (s), 1,361 (s), 1,261 (s), 1,154 (w), 1,129 (w), 1,077 (w), 909 (m), 889 (s), 818 (s), 807 (s), 667 (s), 630 (m), 594 (s), 507 (s).

Synthesis of $Fe_{0.1}Mg_{1.9}$(dobdc) (3). In a 500-ml Schlenk flask, H_4(dobdc) (1.8 g, 8.8 mmol), $MgCl_2$ (1.5 g, 15 mmol) and $FeCl_2$ (0.84 g, 6.6 mmol) were dissolved in a mixture of 310 ml dimethylformamide (DMF) and 40 ml methanol. The reaction was stirred vigorously at 120 °C for 16 hours. The precipitate was filtered and stirred with 250 ml fresh DMF at 120 °C for three hours. Two more DMF washes at 120 °C were performed, after which the precipitate was filtered and soaked in methanol at 60 °C. The methanol exchanges were repeated until no DMF stretches were apparent in the infrared spectrum. The framework was desolvated fully under dynamic vacuum (<15 μbar) at 210 °C for two days to afford $Fe_{0.1}Mg_{1.9}$(dobdc) as a bright yellow–green solid (2.0 g, 8.2 mmol, 93% yield). The iron-to-magnesium ratio was determined by inductively coupled plasma optical emission spectrometry. Analytical: $C_8H_2Fe_{0.1}Mg_{1.9}O_6$ calculated, C, 39.08, H, 0.82; found, C, 39.37, H, 0.43. Infrared (solid ATR) spectroscopy: 1,577 (s), 1,484 (m), 1,444 (s), 1,429 (s), 1,372 (s), 1,236 (s), 1,210 (s), 1,123 (m), 911 (m), 892 (s), 828 (s), 820 (s), 631 (s), 584 (s), 492 (s).

Reactivities of Fe_2(dobdc) (1) and $Fe_{0.1}Mg_{1.9}$(dobdc) (3) with N_2O and C_2H_6. In a typical flow-through experiment, a mixture of gases (2 ml min^{-1} N_2O, 10 ml min^{-1} C_2H_6 and 8 ml min^{-1} Ar for a total flow 20 ml min^{-1}) was flowed over a packed bed of MOF (50–100 mg) contained within a glass column. The column was heated to 75 °C for 24 hours, after which the products were extracted with CD_3CN (3 × 1 ml) and analysed by ^{1}H NMR spectroscopy using 1,4-dichlorobenzene as an internal standard. Although a cold bath maintained at −78 °C was installed downstream of the glass reactor to collect condensable organic products, at the temperatures tested all the products appeared to remain bound to the framework.

In a typical batch experiment, a Parr bomb was charged with N_2O (1.5 bar) and C_2H_6 (7.5 bar) and heated to 75 °C in a sand bath. After 24 hours, the bomb was cooled and the products extracted with CD_3CN.

Electronic structure calculations. The structures of **2** and **4** were optimized using periodic boundary conditions and the PBE + U exchange-correlation functional. From each of these structures, we carved out a model cluster that contained three iron centres along a single helical chain and six organic linkers. These clusters are analogous to the 88-atom cluster model of Fe_2(dobdc) employed previously[41]. The cluster models were simplified further by substituting the two peripheral iron(II) centres with zinc(II) centres, keeping only the central iron(II) in the cluster. Constrained geometry optimizations were performed in which only the central iron and the six oxygen atoms (plus the hydroxide hydrogen in compound **2**) of its first coordination sphere were allowed to relax. Single-point multiconfigurational complete active space (CASSCF) calculations followed by second-order perturbation theory (CASPT2) were performed at PBE-optimized geometries of the cluster models of **2** and **4**, and M06 calculations were performed at M06-L geometries. Full computational details are in the Supplementary Information.

Received 17 December 2013; accepted 14 April 2014; published online 18 May 2014; corrected online 5 June 2014

References

1. Arakawa, H. *et al.* Catalysis research of relevance to carbon management: progress, challenges, and opportunities. *Chem. Rev.* **101,** 953–996 (2001).
2. Bergman, R. G. Organometallic chemistry: C–H activation. *Nature* **446,** 391–393 (2007).
3. International Energy Agency *World Energy Outlook Special Report 2011* http://www.worldenergyoutlook.org/goldenageofgas (2011).
4. Himes, R. A. & Karlin, K. D. Copper–dioxygen complex mediated C–H bond oxygenation: relevance for particulate methane monooxygenase (pMMO). *Curr. Opin. Chem. Biol.* **13,** 119–131 (2009).
5. Costas, M., Mehn, M. P., Jensen, M. P. & Que, L. Jr. Dioxygen activation at mononuclear nonheme iron active sites: enzymes, models, and intermediates. *Chem. Rev.* **104,** 939–986 (2004).
6. Meunier, B., de Visser, S. P. & Shaik, S. Mechanism of oxidation reactions catalyzed by cytochrome P450 enzymes. *Chem. Rev.* **104,** 3947–3980 (2004).
7. Wallar, B. J. & Lipscomb, J. D. Dioxygen activation by enzymes containing binuclear non-heme iron clusters. *Chem. Rev.* **96,** 2625–2658 (1996).
8. Hohenberger, J., Ray, K. & Meyer, K. The biology and chemistry of high-valent iron–oxo and iron–nitrido complexes. *Nature Commun.* **3,** 720 (2012).
9. Nam, W. High-valent iron(IV)–oxo complexes of heme and non-heme ligands in oxygenation reactions. *Acc. Chem. Res.* **40,** 522–531 (2007).
10. Que, L. Jr The road to non-heme oxoferryls and beyond. *Acc. Chem. Res.* **40,** 493–500 (2007).
11. Watton, S. P., Taylor, C. M., Kloster, G. M. & Bowman, S. C. Coordination complexes in sol–gel silica materials. *Prog. Inorg. Chem.* **51,** 333–420 (2002).
12. Leadbeater, N. E. & Marco, M. Preparation of polymer-supported ligands and metal complexes for use in catalysis. *Chem. Rev.* **102,** 3217–3274 (2002).
13. Panov, G. I. *et al.* Iron complexes in zeolites as a new model of methane monooxygenase. *React. Kinet. Catal. Lett.* **61,** 251–258 (1997).
14. Zecchina, A., Rivallan, M., Berlier, G., Lamberti, C. & Richhiardi, G. Structure and nuclearity of active sites in Fe-zeolites: comparison with iron sites in enzymes and homogeneous catalysts. *Phys. Chem. Chem. Phys.* **9,** 3483–3499 (2007).
15. Yoon, J. W. *et al.* Controlled reducibility of a metal–organic framework with coordinatively unsaturated sites for preferential gas sorption. *Angew. Chem. Int. Ed.* **49,** 5949–5952 (2010).
16. Ma, S., Yuan, D., Chang, J-S. & Zhou, H-C. Investigation of gas adsorption performances and H_2 affinities of porous metal–organic frameworks with different entatic metal centers. *Inorg. Chem.* **48,** 5398–5402 (2009).
17. Sumida, K. *et al.* Hydrogen storage and carbon dioxide capture in an iron-based sodalite-type metal–organic framework (Fe–BTT) discovered *via* high-throughput methods. *Chem. Sci.* **1,** 184–191 (2010).
18. Bloch, E. D. *et al.* Selective binding of O_2 over N_2 in a redox-active metal–organic framework with open iron(II) coordination sites. *J. Am. Chem. Soc.* **133,** 14814–14822 (2011).
19. Bloch, E. D. *et al.* Hydrocarbon separations in a metal–organic framework with open iron(II) coordination sites. *Science* **335,** 1606–1610 (2012).
20. Märcz, M., Johnsen, R. E., Dietzel, P. D. C. & Fjellvåg, H. The iron member of the CPO-27 coordination polymer series: synthesis, characterization, and intriguing redox properties. *Micropor. Mesopor. Mater.* **157,** 62–74 (2012).
21. Bhattacharjee, S. *et al.* Solvothermal synthesis of Fe-MOF-74 and its catalytic properties in phenol hydroxylation. *J. Nanosci. Nanotechnol.* **10,** 135–141 (2010).
22. Tolman, W. B. Binding and activation of N_2O at transition-metal centers: recent mechanistic insights. *Angew. Chem. Int. Ed.* **49,** 1018–1024 (2010).
23. Piro, N. A., Lichterman, M. F., Harman, W. H. & Chang, C. J. A structurally characterized nitrous oxide complex of vanadium. *J. Am. Chem. Soc.* **133,** 2108–2111 (2011).
24. Zhao, Y. & Truhlar, D. G. The M06 suite of density functionals for main group thermochemistry, thermochemical kinetics, noncovalent interactions, excited states, and transition elements: two new functionals and systematic testing of four M06-class functionals and 12 other functionals. *Theor. Chem. Acc.* **120,** 215–241 (2008).

25. Delabie, A., Vinckier, C., Flock, M. & Pierloot, K. Evaluating the activation barriers for transition metal N_2O reactions. *J. Phys. Chem. A* **105,** 5479–5485 (2001).
26. Heyden, A., Peters, B. & Bell, A. T. Comprehensive DFT study of nitrous oxide decomposition over Fe-ZSM-5. *J. Phys. Chem. B.* **109,** 1857–1873 (2005).
27. Bottomley, F. & Brooks, W. V. F. Mode of bonding of dinitrogen oxide (nitrous oxide) in (dinitrogenoxide)pentaammineruthenium. *Inorg. Chem.* **16,** 501–502 (1977).
28. Pamplin, C. B., Ma, E. S. F., Safari, N., Rettig, S. J. & James, B. R. The nitrous oxide complex, $RuCl_2(\eta^1\text{-}N_2O)(P\text{–}N)(PPh_3)$ (P–N=[*o*-(*N*,*N*-dimethylamino)phenyl]diphenylphosphine); low temperature conversion of N_2O to N_2 and O_2. *J. Am. Chem. Soc.* **123,** 8596–8597 (2001).
29. Paulat, F. *et al.* Spectroscopic properties and electronic structure of pentammineruthenium(II) dinitrogen oxide and corresponding nitrosyl complexes: binding mode of N_2O and reactivity. *Inorg. Chem.* **43,** 6979–6994 (2004).
30. Reed, A. E., Curtiss, L. A. & Weinhold, F. Intermolecular interactions from a natural bond orbital, donor–acceptor viewpoint. *Chem. Rev.* **88,** 899–926 (1998).
31. Macbeth, C. E. *et al.* O_2 activation by nonheme iron complexes: a monomeric Fe(III)–oxo complex derived from O_2. *Science* **289,** 938–941 (2000).
32. Dolphin, D. H., Sams, J. R., Tsin, T. B. & Wong, K. L. Mössbauer–Zeeman spectra of some octaethylporphyrinato- and tetraphenylporphinatoiron(III) complexes. *J. Am. Chem. Soc.* **100,** 1711–1718 (1978).
33. Que, L. Jr & True, A. E. Dinuclear iron- and manganese-oxo sites in biology. *Prog. Inorg. Chem.* **38,** 97–200 (1990).
34. Soo, H. S., Komor, A. C., Iavarone, A. T. & Chang, C. J. A hydrogen-bond facilitated cycle for oxygen reduction by an acid- and base-compatible iron platform. *Inorg. Chem.* **48,** 10024–10035 (2009).
35. Laarhoven, L. J. J., Mulder, P. & Wayner, D. D. M. Determination of bond dissociation enthalpies in solution by photoacoustic calorimetry. *Acc. Chem. Res.* **32,** 342–349 (1999).
36. Goldsmith, C. R., Jonas, R. T. & Stack, T. D. P. C–H bond activation by a ferric methoxide complex: modeling the rate-determining step in the mechanism of lipoxygenase. *J. Am. Chem. Soc.* **124,** 83–96 (2002).
37. Goldsmith, C. R. & Stack, T. D. P. Hydrogen atom abstraction by a mononuclear ferric hydroxide complex: insights into the reactivity of lipoxygenase. *Inorg. Chem.* **45,** 6048–6055 (2006).
38. Starokon, E. V., Parfenov, M. V., Pirutko, L. V., Abornev, S. I. & Panov, G. I. Room-temperature oxidation of methane by α-oxygen and extraction of products from the FeZSM-5 surface. *J. Phys. Chem. C* **115,** 2155–2161 (2011).
39. Perdew, J. P., Burke, K. & Ernzerhof, M. Generalized gradient approximation made simple. *Phys. Rev. Lett.* **77,** 3865–3868 (1996).
40. Franchini, C. *et al.* Maximally localized Wannier functions in $LaMnO_3$ within PBE+U, hybrid functionals and partially self-consistent GW: an efficient route to construct *ab initio* tight-binding parameters for eg perovskites. *J. Phys. Condens. Mater.* **24,** 235602/1-17 (2012).
41. Verma, P., Xu, X. & Truhlar, D. G. Adsorption on Fe-MOF-74 for C1–C3 hydrocarbon separation. *J. Phys. Chem. C* **117**, 12648–12660 (2013).
42. Maurice, R. *et al.* Single-ion magnetic anisotropy and isotropic magnetic couplings in the metal–organic framework Fe_2(dobdc). *Inorg. Chem.* **52,** 9379–9389 (2013).
43. Andersson, K., Malmqvist, P-Å. & Roos, B. O. Second order perturbation theory with a complete active space self-consistent field reference function. *J. Chem. Phys.* **96,** 1218–1226 (1992).
44. Andersson, K., Malmqvist, P. A., Roos, B. O., Sadlej, A. J. & Wolinski, K. Second-order perturbation theory with a CASSCF reference function. *J. Phys. Chem.* **94,** 5483–5488 (1990).
45. Shaik, S., Hirao, H. & Kumar, D. Reactivity of high-valent iron–oxo species in enzymes and synthetic reagents: a tale of many states. *Acc. Chem. Res.* **40,** 532–542 (2007).
46. England, J. *et al.* The crystal structure of a high-spin oxoiron(IV) complex and characterization of its self-decay pathway. *J. Am. Chem. Soc.* **132,** 8635–8644 (2010).
47. Lacy, D. C. *et al.* Formation, structure, and EPR detection of a high spin Fe^{IV}–oxo species derived from either an Fe^{III}–oxo or Fe^{III}–OH complex. *J. Am. Chem. Soc.* **132,** 12188–12190 (2010).
48. England, J. *et al.* A more reactive trigonal–bipyramidal high-spin oxoiron(IV) complex with a *cis*-labile site. *J. Am. Chem. Soc.* **133,** 11880–11883 (2011).
49. Bigi, J. P. *et al.* A high-spin iron(IV)–oxo complex supported by a trigonal nonheme pyrrolide platform. *J. Am. Chem. Soc.* **134,** 1536–1542 (2012).
50. Pestovsky, O. *et al.* Aqueous Fe^{IV}=O: spectroscopic identification and oxo-group exchange. *Angew. Chem. Int. Ed.* **44,** 6871–6874 (2005).

Acknowledgements

Synthesis, basic characterization experiments and all of the theoretical work were supported by the US Department of Energy, Office of Basic Energy Sciences, Division of Chemical Sciences, Geosciences, and Biosciences under award DE-FG02-12ER16362. Reactivity studies were supported by the Laboratory Directed Research and Development Program of Lawrence Berkeley National Laboratory under US Department of Energy Contract No. DE-AC02-05CH11231. Work at the Molecular Foundry, and XAS experiments performed at the Advanced Light Source (BL 10.3.2), Berkeley, were supported by the Office of Science, Office of Basic Energy Sciences, of the US Department of Energy under Contract No. DE-AC02-05CH11231. X-ray diffraction experiments were performed at the Advanced Photon Source at Argonne National Laboratory (17-BM-B). Use of the Advanced Photon Source, an Office of Science User Facility operated for the US Department of Energy (DOE) Office of Science by Argonne National Laboratory, was supported by the US DOE under Contract No. DE-AC02-06CH11357. S.B., F.B. and V.C. acknowledge financial support from the Ateneo Project 2011 ORTO11RRT5. We also thank the National Science Foundation for providing graduate fellowship support (D.J.X. and J.A.M.). In addition, we are grateful for the support of E.D.B. through a Gerald K. Branch fellowship in chemistry, P.V. through a Phillips 66 Excellence Fellowship and M.R.H. through the National Institute of Standards and Technology/National Research Council Fellowship Program. We thank S. Chavan for help with the infrared spectroscopy experiments and fruitful discussion.

Author contributions

D.J.X., E.D.B. and J.R.L. planned and executed the synthesis, characterization and reactivity studies. J.A.M., W.L.Q., M.R.H. and C.M.B. analysed the powder neutron and X-ray diffraction data. N.P. and P.V. performed the cluster DFT calculations. J.B. and K.L. performed the periodic DFT calculations. A.L.D. performed the CASSCF/PT2 calculations. D.G.T. and L.G. conceived and managed the computational efforts. F.B., V.C. and S.B. carried out the *in situ* transmission Fourier transform infrared studies, and J.Y. supervised EXAFS analysis. All authors participated in the preparation of the manuscript.

Additional information

Supplementary information is available in the online version of the paper. Reprints and permissions information is available online at www.nature.com/reprints. Correspondence and requests for materials should be addressed to J.R.L.

Competing financial interests

The authors declare no competing financial interests.